ChemComm

COMMUNICATION

View Article Online
View Journal | View Issue

Cite this: *Chem. Commun.*, 2020, **56**, 2937

Received 20th January 2020,
Accepted 23rd January 2020

DOI: 10.1039/d0cc00543f

rsc.li/chemcomm

Colloidal synthesis of porous red phosphorus nanoparticles as a metal-free electrocatalyst for the hydrogen evolution reaction†

Cheng-Ying Chan,‡ Chao-Hung Chang‡ and Hsing-Yu Tuan *

Porous red phosphorus nanoparticles, P-RPNPs, were synthesized *via* a new colloidal approach and used as metal-free electrocatalysts in the hydrogen evolution reaction (HER). P-RPNPs were highly efficient in acidic media, required an overpotential of only 218 mV to reach 10 mA cm^{-2}, and exhibited superior long-term durability.

Hydrogen has been regarded as a promising future energy source owing to advantages such as the highest gravimetric energy density[1] and the possibility of zero CO_2 emissions.[2] The hydrogen evolution reaction (HER), which is a cathodic reaction of water electrolysis, provides a promising pathway to sustainable hydrogen production. To drive the reaction with low overpotential, Pt-based materials and Pt alloys are the most efficient HER electrocatalysts because they can initiate proton reduction with small overpotential and enhance the kinetics of the HER, which provides high exchange current densities and efficient activity.[3,4] However, the low abundance and high cost hinder their large-scale applications. Therefore, the development of cost-effective alternative catalysts (*e.g.*, chalcogenides,[5] carbides,[6] nitrides,[7] borides,[8] phosphides,[9] and metal-free materials[10–12]) is important.

Metal-free catalysts may reduce the environmental impact by avoiding metal ion release.[10] Although considerable efforts have been made to develop carbon-based materials owing to their advantages of tunable molecular structures and designated catalysis,[13] little attention is paid to other promising metal-free catalysts. Carbon-based metal-free materials such as graphitic carbon nitride, C_3N_4, coupled with different elements (P, S, N)[14,15] that are doped or co-doped, and carbon nanotubes could be HER catalysts.[16] However, the HER activity of metal-free materials is challenged by metal impurities (*e.g.*, Fe, Co, and Ni; usually 1–10 wt%) because their synthesis may involve metals acting as seeds and dopants.[17]

The P element is 6000 times more abundant than platinum.[18] Among three different types of phosphorus allotropes (*e.g.*, red, white, and black), red phosphorus (RP) is promising owing to its chemical stability and non-toxicity. Besides, RP is easy to manufacture and is inexpensive compared to the other two P allotropes. Recent studies showed that red phosphorus nanoparticles can be synthesized from PI_3 reduced by glycol; it has been determined that the conductivity of iodine doped red phosphorus nanoparticles is much higher than that of commercial RP, which is used in the battery field.[19] Nevertheless, these phosphorus nanoparticles are hydrophilic, which makes them unstable during water splitting. Hydrophilic phosphorus nanoparticles will be well-dissolved after only 10 s of sonication in 0.5 M H_2SO_4 as shown in Fig. S1 (ESI†).

In this communication, we propose to use porous red phosphorus nanoparticles (P-RPNPs) as a new efficient electrocatalyst in the HER field. P-RPNPs possess high activity (at 218 mV, they achieve 10 mA cm^{-2}) and impressive endurance during cycling [6000 cyclic voltammetry (CV) sweeps from −0.6 to 0.2 V (*vs.* RHE)] and durability [at −0.5 V (*vs.* RHE) for 45 h] tests. P-RPNPs showed electrocatalytic HER activity that was comparable to that of carbon-based metal-free materials and some metallic catalysts such as MoS_2 nanomaterials. The abovementioned results provide a new direction for developing Pt-free materials as metal-free electrocatalysts in the HER.

In Fig. 1, a one-pot hot injection approach is developed to obtain monodispersed porous red phosphorus nanoparticles, P-RPNPS. The precursor, phosphorus iodide (P_xI_y), is formed by the reaction between iodine and bulk RP under an argon atmosphere. 1,3-Dimethyl-2-imidazolidinone (DMI) was used to reduce P_xI_y to P-RPNPs. Oleic acid (OA) was also added as a

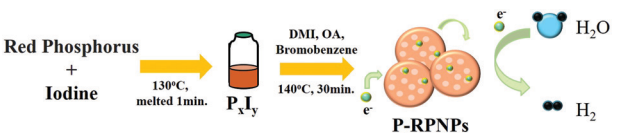

Fig. 1 Schematic diagram of the colloidal synthesis of P-RPNPs and the HER application.

Department of Chemical Engineering, National Tsing Hua University, Hsinchu 30013, Taiwan, P. R. China. E-mail: hytuan@che.nthu.edu.tw

† Electronic supplementary information (ESI) available. See DOI: 10.1039/d0cc00543f

‡ These authors contributed equally to this work.

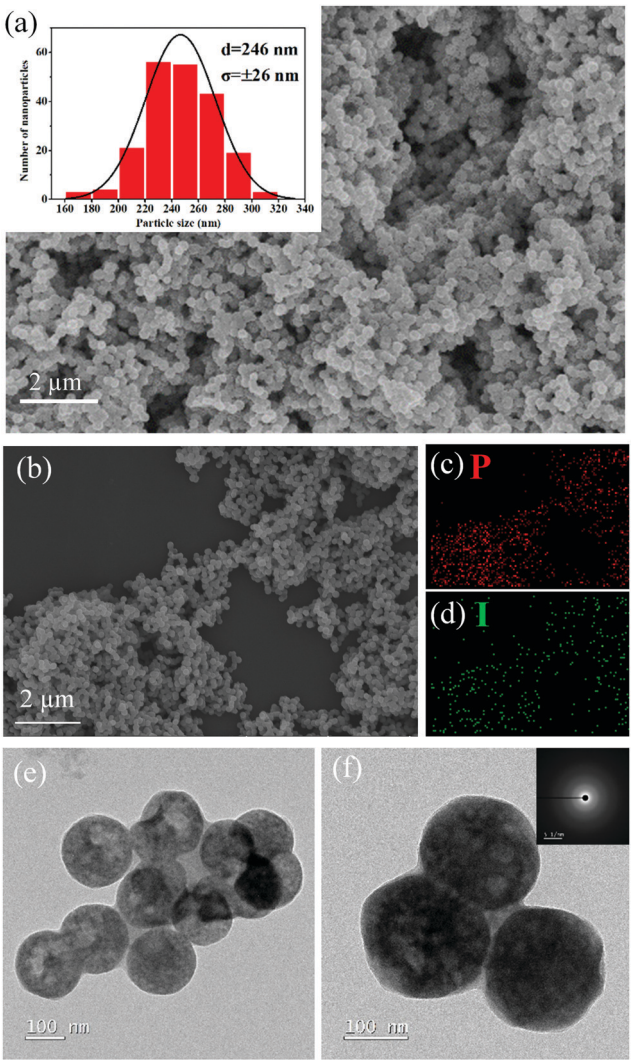

Fig. 2 (a–d) SEM measurement of P-RPNPs. (a) SEM image of P-RPNPs; the inset shows the histograms of size distribution. (b) SEM image of P-RPNPs. (c) EDS with P element mapping by Kα emission peaks and (d) EDS with I element mapping by Lα emission peaks; both elemental mappings correspond to image (b); (e) TEM image of P-RPNPs. (f) TEM images of P-RPNPs with an inset illustrating the SAED pattern.

surfactant, which was essential for the shape control of P-RPNPs. P-RPNPs were synthesized by decomposing the precursor with a solution-phase approach (Synthesis ESI†). The morphology and structure of the synthesized P-RPNPs were examined by SEM and TEM measurements. The average diameter of the P-RPNPs was 246 ± 26 nm, as shown by the histogram of size distribution in Fig. 2(a). Fig. 2(b–d) show the SEM mapping results of P-RPNPs, which demonstrate the uniform distribution of phosphorus and iodine. EDX of RPNPs also shows signals containing carbon (surfactant), phosphorus and iodine (Fig. S2, ESI†). We observed that phosphorus and iodine uniformly exist in the nanoparticles, and the vaporization of iodine at 140 °C might be the reason for porosity. The iodine phase transition phenomenon has been previously reported. Under ordinary atmospheric pressure, in the temperature interval of 113.6–184.4 °C, iodine first melts and then quickly vaporizes owing to its relatively high vapor pressure.[20]

Fig. 2(e and f) show the TEM images of the P-RPNPs, which demonstrate similar particle sizes to those obtained by SEM measurements; in addition, the porous structure was clearly observed in the TEM images. The selected area electron diffraction (SAED) pattern of the P-RPNPs indicated their amorphous structure. In a typical synthesis method for II–VI semiconductor nanoparticles in a solution-phase approach, the surfactants that form nanoparticles in an anisotropic growth can be explained with the effective-monomer model.[21] In the synthesis of nanomaterials, surfactants are the shape-directing agents, for example, gold nanorods require the use of cetyltrimethylammonium bromide (CTAB),[22] and ZnO nanowires require a bond with an amine or a thiol.[23] OA is widely used in nanomaterials, especially for nanoparticles (*e.g.*, SiO_2[24] and Fe_3O_4[25,26]). During the synthesis of nanoparticles, OA molecules chemically adsorb on the nanoparticles, which produces OA-coated nanoparticles; this results in stably monodispersed nanoparticles. However, the detailed mechanism of oleic acid as the surfactant is still unknown, and other widely-used surfactants (*i.e.*, 1-dodecanthiol and oleylamine) cannot replace OA (Fig. S3, ESI†).

Fig. 3 shows the Brunauer–Emmett–Teller (BET) measurements. The specific surface area was obtained, and the pore size distribution was calculated from the corrected form of the Kelvin equation referring to the Barrett–Joyner–Halenda method based on the adsorption branches of the isotherms. The results of the measurements are as follows: BET surface area: 3.3793 $m^2 g^{-1}$ and the average pore size: 210.2 Å. The pore size result is consistent with the pores observed in TEM images with a 100 nm scale bar, as shown in Fig. 2(e and f). Surface area provides active sites for the catalysts. Theoretically, a decrease in the nanomaterial diameter produces more active sites and results in an effective catalyst. P-RPNPs are nanosized, and iodine doped in the material may be the key point highly enhancing the conductivity. As mentioned in some published reports[19,27–29] iodine doped carbon nanotubes own specific conductivity higher than copper and aluminum and iodine-doped sulfurized polyacrylonitrile enhancing the conductivity of the material. Therefore, P-RPNPs exhibit a much higher electroactivity than RP. Furthermore, P-RPNPs have nanosized

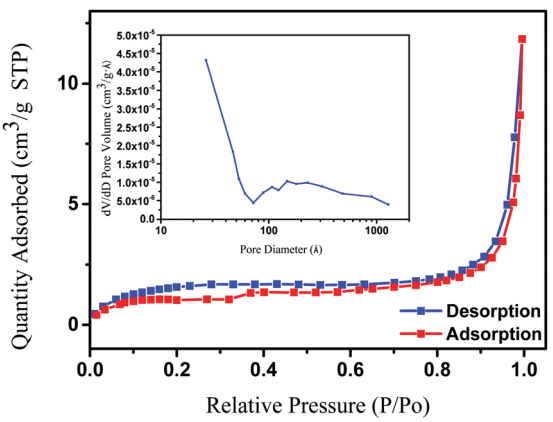

Fig. 3 N_2 adsorption–desorption isotherms of P-RPNP powders. The inset shows the corresponding pore size distribution.

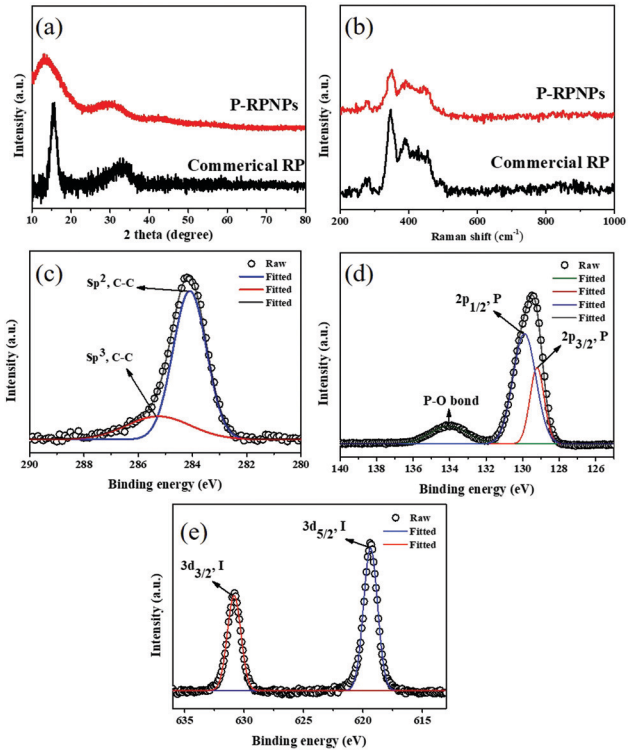

Fig. 4 (a) XRD patterns of P-RPNPs and commercial red phosphorus. (b) Raman spectra of P-RPNPs. (c–e) XPS spectra of P-RPNP samples: (a) C: sp^2, sp^3 (b) P: 2p (c) I: 3d.

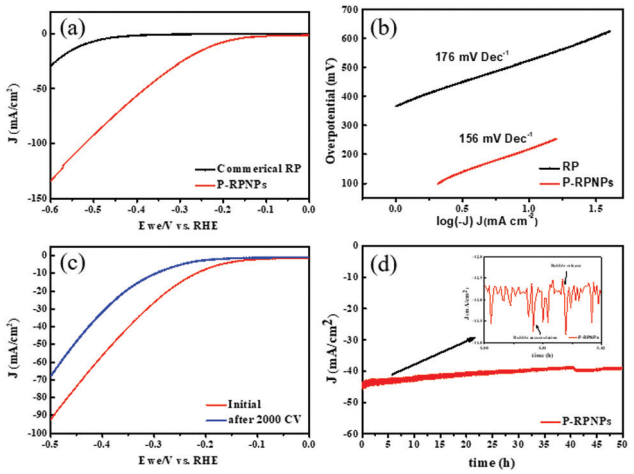

Fig. 5 (a) HER polarization curves of P-RPNPs, commercial RP, and wet ball-milled commercial RP in 0.5 M H_2SO_4 from 0.0 V to −0.6 V at 5 mV s^{-1} with no IR compensation. (b) Corresponding Tafel plots for P-RPNPs and commercial RP. (c) HER durability test for the P-RPNP catalyst at the voltage from 0.2 to −0.6 V for 2000 cycles in 0.5 M H_2SO_4. (d) P-RPNP stability test at the current density of −0.5 V (*vs.* RHE) for 50 h.

pores that range from 10 to 30 nm and offer additional surface area; thus, P-RPNPs are novel nanomaterials that can be applied in the HER.

Fig. 4(a and b) show the XRD and Raman spectra of solid P-RPNPs. The XRD pattern of P-RPNPs has three broad diffraction peaks ranging from 11 to 16°, 26 to 36° and 47 to 65° respectively, which agree well with the XRD pattern of commercial RP and other amorphous red phosphorus nanoparticles.[19,30] The XPS spectra of P-RPNPs are shown in Fig. 4(c–e); the binding energies at 284.1 eV and 285.3 eV correspond to sp^2 and sp^3-hybridized carbon. For P-RPNPs, the binding energies at 129.2 eV and 129.9 eV correspond to $2p_{3/2}$ and $2p_{1/2}$ of phosphorus, respectively. In addition, owing to the oxidation in the air, we also observed P–O bonding at 134.0 eV; the binding energies of 619.4 eV and 630.8 eV are indicative of $3d_{5/2}$ and $3d_{3/2}$ of iodine, respectively. Thus, on the basis of XPS and SEM measurements, we can confirm that we prepared P-RPNPs.

The electrolysis of water produces high purity hydrogen using an eco-friendly method. Next, the HER ($2H_{(aq)} + 2e^- \rightarrow H_{2(g)}$) activity of P-RPNPs as an electrocatalyst is evaluated. P-RPNPs were deposited on a glassy carbon electrode, and 0.5 M H_2SO_4 was used as an electrolyte in a typical three-electrode system. To attach P-RPNPs to the working electrode, the as-synthesized nanoparticles were dispersed in a toluene solution and formed an ink with a concentration of 3 mg mL^{-1}. The area of the working electrode was 0.196 cm^2 and was prepared by directly depositing ink on the electrode (~0.3 mg cm^{-2}).

Linear sweep voltammetry (LSV) measurement was carried out to measure the HER electrocatalyst. At a geometrical catalytic current density of 10 mA cm^{-2}, P-RPNPs showed an overpotential as low as 218 mV [Fig. 5(a)], which is comparable to that of carbon materials for the same current density standard. For example, the overpotential for oxidized carbon nanotubes[10] is 220 mV and that for C_3N_4 nanoribbons on graphene nanosheets[31] is 207 mV. In addition, in this experiment, we confirmed that phosphorus nanoparticles considerably enhance the performance of the HER catalyst. For commercial RP, the overpotential is 523 mV at the current density of 10 mA cm^{-2}. SEM images of commercial RP are shown in Fig. S9 and S10, ESI.† In addition, we compare the overpotential of P-RPNPs at the current density of 10 mA cm^{-2} with that of other metal-free catalysts as shown in Table S1, ESI.† In addition, P-RPNPs also exhibited a considerable performance compared to the HER activities of various types of materials. The overpotential for metal-free materials at the current density of 10 mA cm^{-2} is approximately 200–425 mV;[17] P-RPNPs performed well in this range. Furthermore, the performance of P-RPNPs is also comparable to that of some metallic materials, such as MoS_2 nanosheets[32] at approximately 205 mV overpotential. Moreover, Tafel plots are typically used to predict the rate determining steps and mechanism of the electrochemical process of the HER. The Tafel slope results were determined to be approximately 176 mV dec^{-1} and 156 mV dec^{-1}, and both were over 120 mV dec^{-1}; thus, they exhibited neither a Heyrovsky nor Volmer reaction mechanism in the HER and were supposed to be diffusion-controlled.[10,33] The electrochemical impedance spectroscopy (EIS) measurements of P-RPNPs were carried out in the potentiostatic mode at the potential of −0.12 V (*vs.* RHE) with a scanning frequency of 10^5–0.01 Hz (Fig. S10, ESI†). P-RPNP showed a lower overpotential in the EIS measurements than that of commercial RP, which resulted in higher conductivity and lower

overpotential; these observations were in agreement with the LSV results.

Another key factor for HER catalysts is durability,[34,35] which links the catalyst life span and activity, and provides an important indicator for evaluating practical applications. P-RPNPs showed an excellent durability performance. The long-term durability was also examined under a static potential at −0.5 V (*vs.* RHE) for 45 h. As shown in Fig. S9 (ESI†), after 6000 CV sweeps from −0.6 V to 0.2 V with a scan rate of 100 mV s^{-1} without IR compensation, the P-RPNPs still maintained *I–V* curves that were similar to the previous one obtained in the initial test and the cathodic current densities remained stable. For efficient HER electrocatalysts, the demonstration of long-term durability in an acidic medium is rarely discovered or reported.[36] On the basis of the above evidence mentioned, the combination of high activity and superior durability indicates the high potential of P-RPNPs.

In this study, we are the first to demonstrate the use of red phosphorus as an electrocatalyst in the HER and describe a novel colloidal approach for synthesizing monodispersed P-RPNPs as metal-free nanomaterials for use as a HER electrocatalyst, and the metal-free feature is well supported by solid experimental evidence (Fig. S11, S15 and Table S2, ESI†). The P-RPNPs exhibited superior activity and long-term durability in an acidic medium. The HER activity of the P-RPNPs based on 10 mA cm^{-2} is much better than bulk red phosphorus and comparable to other metal-free catalysts including carbon-based materials and even some metallic catalysts such as MoS_2 nanosheets. The proposed synthesis method is valuable for other nanomaterials and the high abundance of phosphorus could open up a new avenue for electrocatalyst development and its application in the HER.

We acknowledge the financial support by the Ministry of Science and Technology, Taiwan, through the grants of MOST 106-2622-8-007-017 and MOST 108-2636-E-007-013 and by National Tsing Hua University through the grant of 107Q2708E1.

Conflicts of interest

There are no conflicts to declare.

Notes and references

1 P. P. Edwards, V. L. Kuznetsov and W. I. F. David, *Philos. Trans. R. Soc., A*, 2007, **365**(1853), 1043–1056.
2 N. Muradov, *Int. J. Hydrogen Energy*, 2017, **42**(20), 14058–14088.
3 B. Conway and B. Tilak, *Electrochim. Acta*, 2002, **47**(22-23), 3571–3594.
4 Y. Zhao, F. Zhao, X. Wang, C. Xu, Z. Zhang, G. Shi and L. Qu, *Angew. Chem., Int. Ed.*, 2014, **53**(50), 13934–13939.
5 J. McAllister, N. A. Bandeira, J. C. McGlynn, A. Y. Ganin, Y. F. Song, C. Bo and H. N. Miras, *Nat. Commun.*, 2019, **10**(1), 370.
6 S. Jing, L. Zhang, L. Luo, J. Lu, S. Yin, P. K. Shen and P. Tsiakaras, *Appl. Catal., B: Environ.*, 2018, **224**, 533–540.
7 F. Song, W. Li, J. Yang, G. Han, P. Liao and Y. Sun, *Nat. Commun.*, 2018, **9**, 4531.
8 A. Wang, L. Shen, M. Zhao, J. Wang, W. Li, W. Zhou, Y. Feng and H. Liu, *J. Mater. Chem. C*, 2019, **7**, 8868–8873.
9 M. Q. Wang, C. Ye, H. Liu, M. Xu and S. J. Bao, *Angew. Chem., Int. Ed.*, 2018, **57**(7), 1963–1967.
10 W. Cui, Q. Liu, N. Cheng, A. M. Asiri and X. Sun, *Chem. Commun.*, 2014, **50**(66), 9340–9342.
11 J. X. Feng, H. Xu, S. H. Ye, G. Ouyang, Y. X. Tong and G. R. Li, *Angew. Chem., Int. Ed.*, 2017, **56**(28), 8120–8124.
12 Y. Ito, W. Cong, T. Fujita, Z. Tang and M. Chen, *Angew. Chem., Int. Ed.*, 2015, **54**(7), 2131–2136.
13 Y. Zheng, Y. Jiao, L. H. Li, T. Xing, Y. Chen, M. Jaroniec and S. Z. Qiao, *ACS Nano*, 2014, **8**(5), 5290–5296.
14 X. Liu, W. Zhou, L. Yang, L. Li, Z. Zhang, Y. Ke and S. Chen, *J. Mater. Chem.*, 2015, **3**(16), 8840–8846.
15 J. Zhang, L. Qu, G. Shi, J. Liu, J. Chen and L. Dai, *Angew. Chem., Int. Ed.*, 2016, **55**(6), 2230–2234.
16 R. Gao, Q. Dai, F. Du, D. Yan and L. Dai, *J. Am. Chem. Soc.*, 2019, **141**(29), 11658.
17 M. Zeng and Y. J. J. o. M. C. A. Li, *J. Mater. Chem. A*, 2015, **3**(29), 14942–14962.
18 H. E. Suess and H. C. Urey, *Rev. Mod. Phys.*, 1956, **28**(1), 53.
19 W.-C. Chang, K.-W. Tseng and H.-Y. Tuan, *Nano Lett.*, 2017, **17**(2), 1240–1247.
20 M. Stojanovska, V. M. Petruševski and B. Šoptrajanov, *Educ. Quim.*, 2012, **23**, 171–174.
21 S. Kumar and T. Nann, *Small*, 2006, **2**(3), 316–329.
22 M. A. Wall, S. Harmsen, S. Pal, L. Zhang, G. Arianna, J. R. Lombardi, C. M. Drain and M. F. Kircher, *Adv. Mater.*, 2017, **29**(21), 1605622.
23 S.-Z. Deng, H.-M. Fan, M. Wang, M.-R. Zheng, J.-B. Yi, R.-Q. Wu, H.-R. Tan, C.-H. Sow, J. Ding and Y.-P. Feng, *ACS Nano*, 2009, **4**(1), 495–505.
24 Z. Li and Y. Zhu, *Appl. Surf. Sci.*, 2003, **211**(1-4), 315–320.
25 L. Zhang, R. He and H.-C. Gu, *Appl. Surf. Sci*, 2006, **253**(5), 2611–2617.
26 D. Li, D. Jiang, M. Chen, J. Xie, Y. Wu, S. Dang and J. Zhang, *Mater. Lett.*, 2010, **64**(22), 2462–2464.
27 Y. Zhao, J. Wei, R. Vajtai, P. M. Ajayan and E. V. Barrera, *Sci. Rep.*, 2011, **1**, 83.
28 J. Zhang, A. Xing, B. Jia and X. Liu, *High Perform. Polym.*, 2019, **31**(8), 893–900.
29 S. Ma, P. Zuo, H. Zhang, Z. Yu, C. Cui, M. He and G. Yin, *Chem. Commun.*, 2019, **55**(36), 5267–5270.
30 J. Qian, X. Wu, Y. Cao, X. Ai and H. J. A. C. I. E. Yang, *Angew. Chem., Int. Ed.*, 2013, **52**(17), 4633–4636.
31 Y. Zhao, F. Zhao, X. Wang, C. Xu, Z. Zhang, G. Shi and L. Qu, *Angew. Chem., Int. Ed.*, 2014, **53**(50), 13934–13939.
32 D. Voiry, M. Salehi, R. Silva, T. Fujita, M. Chen, T. Asefa, V. B. Shenoy, G. Eda and M. J. N. l. Chhowalla, *Nano Lett.*, 2013, **13**(12), 6222–6227.
33 T. Shinagawa, A. T. Garcia-Esparza and K. Takanabe, *Sci. Rep.*, 2015, **5**, 13801.
34 X. Liu, M. Zhang, T. Yang, L. Wang, H. Zhu, S. Wang and M. Du, *Mater. Des.*, 2016, **109**, 162–170.
35 Y.-J. Ko, J.-M. Cho, I. Kim, D. S. Jeong, K.-S. Lee, J.-K. Park, Y.-J. Baik, H.-J. Choi and W.-S. Lee, *Appl. Catal., B*, 2017, **203**, 684–691.
36 J. Deng, P. Ren, D. Deng, L. Yu, F. Yang and X. Bao, *Energy Environ. Sci.*, 2014, **7**(6), 1919–1923.

